

Neutron Scattering Analysis of the *Cryptococcus neoformans* Polysaccharide Reveals Solution Rigidity and Repeating Fractal-like Structural Patterns

Supporting Information

Ziwei Wang¹, Susana C. M. Teixeira^{2,3*}, Camilla Strother¹, Antony Bowen¹, Arturo Casadevall¹, and Radamés JB Cordero^{1*}

¹Molecular Microbiology and Immunology, Johns Hopkins Bloomberg School of Public Health, Baltimore, Maryland, 21205, USA. ²NIST Center of Neutron Research, National Institute of Standards and Technology, Gaithersburg, Maryland, 20899, USA. ³Department of Chemical and Biomolecular Engineering, University of Delaware, Newark, Delaware, 19716, USA. *Corresponding authors.

1- Dynamic light scattering data on the exo-PS sample.

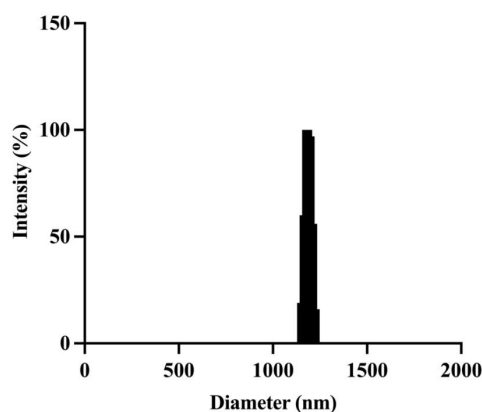


Figure S1. Dynamic light scattering (DLS) analysis of 10 mg/mL exo-PS solution accumulated on a 10 kDa molar mass cutoff membrane. The polydispersity of the exo-PS was 0.355, determined by DLS coupled with a 90Plus/BI-MAS Multi-Angle Particle Sizing analyzer (Brookhaven Instruments Corp., NY, USA).

2- Neutron scattering data on the exo-PS samples, and data fitting.

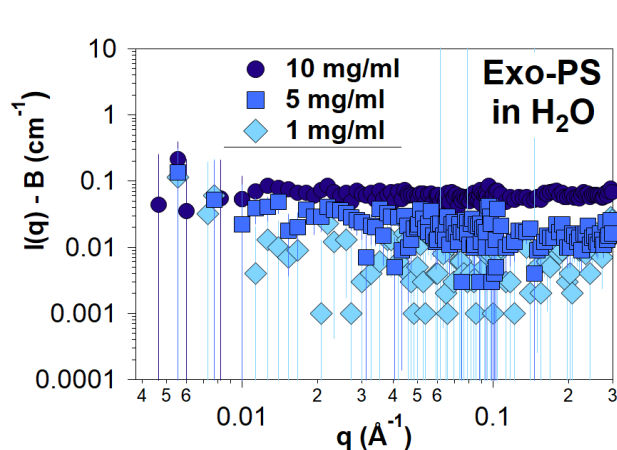


Figure S2. Background subtracted SANS data – data collected for buffer-only solutions was subtracted from the PS-containing samples – measured on exo-PS in H₂O at 30 °C and various concentrations, as labeled. The scattered intensities show approximately flat profiles, indicative of poor contrast for the scattering angles measured. The error bars represent standard errors from counting statistics and when not visible are smaller than the corresponding data marker.

42 Small angle neutron scattering (SANS) data on the exo-PS solutions in D₂O were fitted using
 43 the correlation length model available in SasView¹, as described in the main document, where
 44 the calculated scattered intensities are defined as²:

$$45 \quad I(q) = \frac{A}{q^n} + \frac{C}{1 + (q\xi)^m} + B$$

46
 47 where the first term describes Porod scattering from pore clusters (exponent n) and the second
 48 term is a Lorentzian function describing scattering from polymer chains (exponent m). The
 49 second term characterizes the polymer/solvent interactions, and the two multiplicative factors
 50 A and C are, respectively, the Porod scale and the Lorentz scale. ξ is a correlation length for
 51 the polymer chains, and B is a q -independent incoherent neutron scattering intensity
 52 contribution to $I(q)$. The calculated intensities from the correlation length model were smeared
 53 to match the instrumental pinhole smearing read from the reduced experimental data file. Fits
 54 to the SANS data minimize a statistical parameter that quantifies the differences between
 55 observed (measured) data and theoretical (calculated from the correlation length model) data
 56 points, defined as:

$$57 \quad \chi^2 = \sum \frac{(Y_{obs} - Y_{theor})^2}{weight^2}$$

58
 59 where the weight given to each data point takes into account the counting errors associated
 60 with the measured intensities, read from the data file. The goodness-of-fit was assessed using
 61 a reduced chi-squared parameter, that takes into account the degrees of freedom (the number
 62 of observed points N_{obs} subtracted by the number of fitted parameters N_{fitted}):

$$63 \quad \chi_{red}^2 = \frac{\chi^2}{N_{obs} - N_{fitted}}$$

64
 65
 66
 67 **Table S1.** Fitting parameters for the exo-PS SANS data using a modified correlation length model².
 68 The data were fitted for $0.001 \leq q \text{ (}\text{\AA}^{-1}\text{)} \leq 0.3$. Higher q data were not included to prevent biasing the
 69 fits with data points that are sensitive to background subtraction effects during data reduction. Values
 70 where no uncertainties are shown were kept fixed during the fits.

Exo-PS (D ₂ O)	1 mg/mL	5 mg/mL	10 mg/mL
q-range (\AA^{-1})	0.001 – 0.30	0.001 – 0.30	0.001 – 0.30
Reduced Chi-squared	0.83	1.74	1.00
Volume fraction	0.001	0.005	0.01
Background B (cm^{-1})	0.0012	0.0019	0.0035
Lorentz scale C	2.2 ± 0.5	3.0 ± 0.1	2.0 ± 0.1
Porod scale A	$(3.2 \pm 1.5) \times 10^{-6}$	$(16 \pm 0.3) \times 10^{-6}$	$(18.0 \pm 2.5) \times 10^{-6}$
Correlation length ξ (\AA)	48.9 ± 7.8	48.6 ± 1.1	49.9 ± 1.3
Porod exponent n	3.28 ± 0.16	2.89 ± 0.04	2.91 ± 0.02
Lorentz exponent m	0.79 ± 0.16	1.02 ± 0.03	1.06 ± 0.04

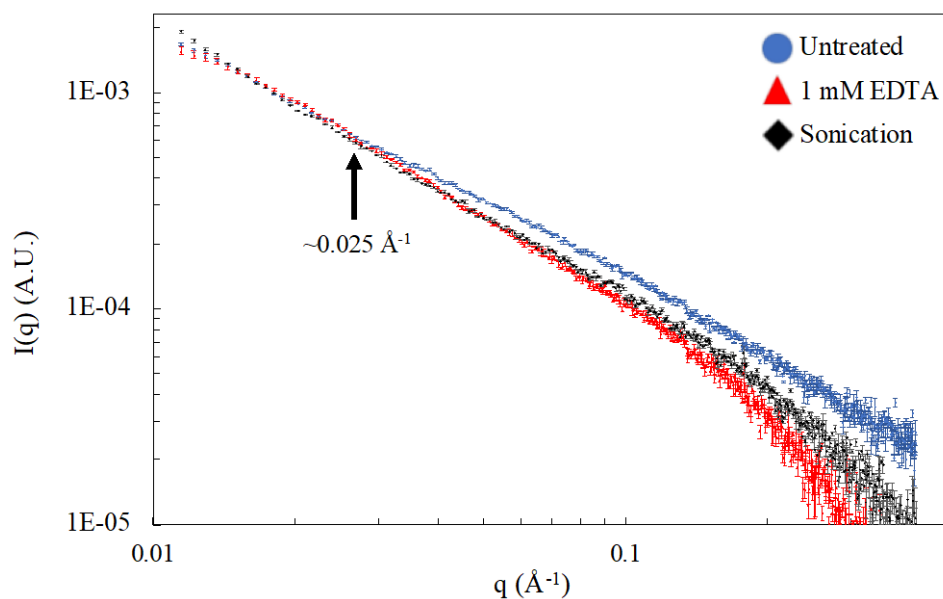
71
 72
 73
 74

75
76
77

3- Small angle X-ray scattering data on exo-PS samples.

78 Preliminary Small Angle X-ray Scattering (SAXS) experiments have been carried out on samples
79 dialyzed against a buffer containing a chelating agent (10 mM NaCl and 1 mM EDTA in H₂O). The
80 data (see Figure S3) was compared for samples prepared in pure water, and samples treated by
81 sonication for 20 minutes prior to data collection (a common protocol used to disaggregate
82 polysaccharides, see for example presented by Geresh *et al.*³).

83 There is insufficient data at low q to accurately measure the q -dependency of the intensities and
84 the scale of the fractal behavior but, compared to exo-PS prepared in water only, the results show a
85 clear shift in the scattering intensities for the EDTA-treated sample, particularly at $q \approx 0.025 \text{ \AA}^{-1}$ and
86 higher, where the data is consistent with significant disaggregation of the polysaccharide (comparable
87 to the effects of sonication). While this preliminary data supports the theory of a strong role for cationic
88 bridging in the structuring of exo-PS, this comparison should take into consideration a few limitations,
89 namely: (1) potentially restricted accessibility of EDTA and solvent to parts of the compact gel network
90 and (2) the known susceptibility of exo-PS to ionizing radiation-induced ablations (that can occur from
91 exposure to X-rays during SAXS measurements), particularly if prior sonication increases free-radical
92 diffusion and accessibility of the polymer⁴. A deeper understanding of the role of cation bridging will
93 require a series of systematic studies using optimized sample treatment protocols to assess and mitigate
94 radiation damage (SAXS), and neutron scattering data (SANS) to prevent potential sample
95 discrepancies.

96
97

98
99 **Figure S3.** SAXS data collected of 10 mg/mL exo-PS samples prepared in pure water, in a buffer
100 containing EDTA as a chelating agent (EDTA treated) and for samples that were sonicated for 20
101 minutes prior to data collection (Sonicated). Buffer contributions have not been subtracted from the
102 shown intensity profiles. The data points are colored as described in the legend. Error bars represent
103 standard errors from counting statistics. Data were collected at the Brazilian Synchrotron Light
104 Laboratory (LNLS) with SAPUCAIA beamline (Scattering APparatUs for Complex Applications and
105 *In-situ* Assays).

106
107
108

109
110
111
112
113
114
115
116**4- Light microscopy, USANS, and SANS data on whole fungal cells**

Table S2 shows estimates of the cell dimensions based on optical microscopy data, as well as estimates of the corresponding radii of gyration R_g , assuming an approximately spherical shape with a uniform distribution of neutron scattering length density. The radius of gyration for a sphere can be estimated from the real-space radius R of the cells by:

$$R_g^2 = \frac{3}{5} R^2$$

117
118
119
120
121

Table S2. Cell dimensions are estimated from optical microscopy data of samples containing whole and gamma-irradiated cells in different buffers, where D is the diameter, V is the volume, R_g is the expected radius of gyration, and T is the thickness.

Cell Samples		Cell			Cell Body		PS Capsule	
		D (μm)	V (μm^3)	R_g (μm)	D (μm)	V (μm^3)	T (μm)	V (μm^3)
Whole	D ₂ O	13.9 ± 2.9	1406	5.4 ± 1.9	5.9 ± 1.8	109	4.0 ± 1.4	1297
	H ₂ O	13.2 ± 3.3	1205	5.0 ± 1.6	5.9 ± 1.5	109	3.6 ± 1.5	1096
Irradiated	D ₂ O	6.3 ± 2.7	135	2.3 ± 1.4	6.4 ± 2.7	134	-	-
	H ₂ O	7.2 ± 2.9	188	2.7 ± 1.5	7.2 ± 2.9	188	-	-

122
123
124
125
126
127
128
129

For both whole and gamma-irradiated cells, the USANS intensities appear to trend towards a plateau value at low q , reflecting the size of the particles in solution. Assuming that there are no significant interactions between the cells at the concentrations used and that the cells are approximately spherical with a uniform distribution of neutron scattering length density, the Guinier approximation is valid for $q \times R_g < 1$:

$$\ln I(q) = \ln I(0) - \frac{q^2 R_g^2}{3}$$

130
131
132
133
134
135
136
137
138

where $I(q)$ are the scattered intensities as a function of the momentum transfer magnitude $q^{5,6}$. Guinier fits for the irradiated cell samples are shown in **Figure S4**. As shown in **Table S3**, although the USANS data captured part of the Guinier regime, given that USANS data were collected for $q > 3 \times 10^{-5} \text{ \AA}^{-1}$, there are insufficient data points in the Guinier regime for the non-irradiated cells.

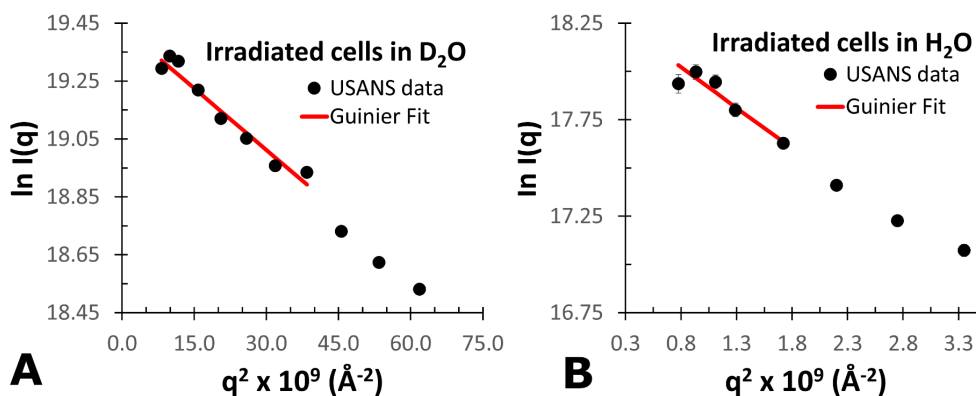
139
140
141
142

Table S3. Parameter fits for the USANS data on the gamma-irradiated cells, where the slit-smearing effects of the experimental resolution were taken into account when performing the Guinier fits, and $I(0)$ is the intensity at zero q . The errors shown report the standard deviation of the parameters (square root of the covariance matrix diagonal elements), and r^2 is the linear regression goodness-of-fit.

Cell samples	R_g (μm)	$I(0)$ $\times 10^8$ (A.U.)	$q \times R_g$	q -range $\times 10^{-5}$ (\AA^{-1})	r^2
Whole, D ₂ O	-	-	< 1	< 1.9	-
Whole, H ₂ O	-	-	< 1	< 2	-
Irradiated, D ₂ O	2.063 ± 0.031	(2.76 ± 0.02)	0.59 - 1.28	3 - 6	0.956
Irradiated, H ₂ O	3.168 ± 0.498	(0.85 ± 0.09)	0.85 - 1.12	3 - 4	0.502

143

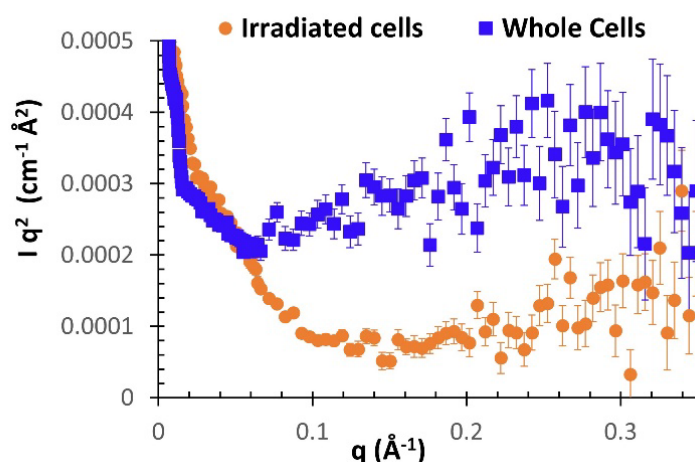
144



145
146 **Figure S4.** Guinier plots and corresponding data fits for the irradiated cell samples in (A) D₂O and (B)
147 H₂O buffers. Error bars represent standard errors from counting statistics and when not visible are
148 smaller than the corresponding data marker.
149
150

151 In the SANS regime, contributions to the scattering from multiple components of the
152 fungal cells preclude a more objective analysis of the data in terms of the structure of the
153 capsular PS. At high- q , however, the differences observed between whole and irradiated
154 samples in the presence of D₂O are consistent with the branched structure of the polysaccharide
155 contributing to scattering from the whole cells, and absent in the irradiated samples. The
156 differences at high- q for whole and irradiated samples are not observed in H₂O, where exo-PS
157 data had already shown that the PS is matched out.

158 A Kratky plot calculated from the scattering data for the solutions in D₂O is shown in
159 Figure S5, where the differences between whole and gamma-irradiated cell samples are
160 highlighted. The Kratky plot does not show the rigid rod-like profile for the irradiated samples.
161 Although it should be highlighted that Kratky plots are extremely sensitive to effects of
162 inconsistencies in background subtraction, and potential contributions from other materials
163 present in the fungal cells cannot be ruled out, the data is consistent with the capsular PS
164 removal from the irradiated cells observed as in the light microscopy images.



165
166 **Figure S5.** Kratky plots calculated from the SANS data collected on fungal cell samples in D₂O. Error
167 bars represent standard errors from counting statistics and when not visible are smaller than the
168 corresponding data marker.
169

170

171 **DISCLAIMER**

172 Certain commercial equipment, software, instruments, and materials are identified to foster
173 understanding. Such identification does not imply recommendation or endorsement by the
174 National Institute of Standards and Technology, nor does it imply that the materials or
175 equipment identified are necessarily the best available for the purpose. The statements,
176 findings, conclusions, and recommendations are those of the authors and do not necessarily
177 reflect the view of NIST or the U.S. Department of Commerce.

178

179 **REFERENCES**

180 (1) *SasView - Small Angle Scattering Analysis*. <https://www.sasview.org/> (accessed 2023-07-
181 26).

182 (2) Hammouda, B.; Ho, D. L.; Kline, S. Insight into Clustering in Poly(Ethylene Oxide)
183 Solutions. *Macromolecules* 2004, 37 (18), 6932–6937. <https://doi.org/10.1021/ma049623d>.

184 (3) Geresh, S.; Adin, I.; Yarmolinsky, E.; Karpasas, M. Characterization of the Extracellular
185 Polysaccharide of Porphyridium Sp.: Molecular Weight Determination and Rheological
186 Properties. *Carbohydr. Polym.* **2002**, 50 (2), 183–189. [https://doi.org/10.1016/s0144-
187 8617\(02\)00019-x](https://doi.org/10.1016/s0144-8617(02)00019-x).

188 (4) Durrani, C. M.; Donald, A. M. Shape, Molecular Weight Distribution and Viscosity of
189 Amylopectin in Dilute Solution. *Carbohydr. Polym.* **2000**, 41 (2), 207–217.
190 DOI:10.1016/s0144-8617(99)00070-3.

191 (5) Serdyuk, I. N.; Tsalkova, T. N.; Svergun, D. I.; Izotova, T. D. Determination of Radii of
192 Gyration of Particles by Small-Angle Neutron Scattering: Calculation of the Effect of
193 Aggregates. *J. Mol. Biol.* **1987**, 194 (1), 126–128. [https://doi.org/10.1016/0022-
194 2836\(87\)90721-2](https://doi.org/10.1016/0022-2836(87)90721-2).

195 (6) Zaccai, G.; Jacrot, B. Small Angle Neutron Scattering. *Annu. Rev. Biophys. Bioeng.* **1983**,
196 12 (1), 139–157. <https://doi.org/10.1146/annurev.bb.12.060183.001035>.